Int. J. Electrochem. Sci., 13 **(2018)** 5195 – 5203, doi: 10.20964/2018.06.48

International Journal of
ELECTROCHEMICAL
SCIENCE
www.electrochemsci.org

Short Communication

Synthesis of Si-SiO_x/rGO/PPy Composite as Anode Material for Li-ion Batteries via in-situ Polymerization Process

Yijuan Zhang[1], *Yurong Ren*[1,*], *Jianning Ding*[1,2,*]

[1] School of Materials Science and Engineering, Jiangsu Collaborative Innovation Center of Photovolatic Science and Engineering, Changzhou University, Changzhou, 213164, Jiangsu, China
[2] Jiangsu Province Cultivation base for State Key Laboratory of Photovoltaic Science and Technology, Changzhou University, Changzhou, 213164, Jiangsu, China
[*]E-mail: ryrchem@163.com, ryrchem@cczu.edu.cn

Received: 3 February 2018 / *Accepted:* 5 April 2018 / *Published:* 10 May 2018

Si-SiO_x/rGO/PPy composite is successfully synthesized via in-situ polymerization process, and then investigated by X-ray diffraction (XRD), scanning electron microscope (SEM),transmission electron microscopy (TEM), infrared Spectroscopy (IR) and charge-discharge test. It is proved that Si-SiO_x/rGO/PPy composite possesses much better electrochemical performance in comparison with Si-SiO_x and Si-SiO_x/rGO composites. It possesses a reversible lithium capacity of 1478.3 $mAh \cdot g^{-1}$ at 100 $mA \cdot g^{-1}$, and 30.4% of its capacity is remained after 70 cycles.

Keywords: Si-SiO_x; rGO; PPy, Anode material; In-situ polymerization

1. INTRODUCTION

Silicon is considered as one of the most attractive candidate anodes for high-energy Li-ion batteries because of its high theoretical capacity, satisfactory operation potential and abundant resources. Unfortunately, the large volume expansion (~400%) upon lithium insertion/extraction in Si during cycling process, usually leads to the breakage of silicon particles and stripping of itself from the current collect, which further severely results in poor cycle performance [1]. So far, a great deal tactics have been suggested to resolve the problems, including synthesis of nanostructured silicon [2–7], coating nanosilicons with conductive materials [8–11] or the dispersion of nanosilicons in buffer matrix. Also, fabrication of Si-SiO_x composites can greatly improve its cycle performances [12-14], owing to the in situ generated Li_2O during the first discharge process, which can inhibit the volume changes of silicon particles during the charge-discharge process [15].

Recently, graphene is frequently introducted into composites with electrode materials, due to its

large surface area, high conductivity, excellent mechanical flexibility [16,17], which will provide a good electrical contact for electrode materials as well as buffer the volume variations during the charge-discharge process [18]. In addition, PPy has been demonstrated as a better conductive polymer to enhance the electrochemical performance of electrode materials for Li-ion batteries, due to its good intrinsic electrochemical performance, the function of accommodating the internal stress of electrode materials and avoiding the dissolution and aggregation of active materials [19-21].

Building on our previous work and the above consideration, Si-SiO_x/rGO/PPy composite was designed by a novel method, and its structural, morphology and electrochemical performance were investigated in detail. The as-obtained sample displayed high specific capacity and cycle stability.

2. EXPERIMENT

Firstly, 0.2 g NaOH was mixed with 6.0 g SiO (45 μm) with 10 mL absolute ethyl alcohol as solvent, and then switched to a tube furnace after drying. Secondly, the mixture was heated to 800℃ at 5℃ min^{-1} under the argon atmosphere, and then remained the temperature of 800℃ for 10 min. Finally, the heated sample was washed with aqueous ammonia (pH = 9.5) for several times, and then dried at 100℃ in vacuum to obtain the Si-SiO_x composite .

Graphite oxide (GO) was prepared by using flake graphite as the starting material via the modified Hummers method according the reported document [22]. The as-obtained graphite oxide was dispersed in deionized water to prepared 2.5 $mg{\cdot}ml^{-1}$ aqueous solution. After that, 80 ml anhydrous ethanol, 40 ml ultrapure water and 0.4 g cetyltrimethyl ammonium bromide (CTAB) was mixed thoroughly after stirring for 60 min, followed by adding 0.4 g Si-SiO_x and magnetic stirring 60 min. then mixed with 80 ml 2.5 $mg{\cdot}ml^{-1}$ above graphite oxide aqueous solution. Subsequently, the mixture was switched into the Teflon-lined autoclaves and kept at 180°C for 10 h. Finally, the mixture was filtrated and dried in vacuum at 60°C for 24 h.

Si-SiO_x/rGO/PPy composite was made via the following solution processes. Firstly, $3.266{\cdot}10^{-3}$ mol pyrrole monomer and 0.1 g Si-SiO_x/rGO was added into 2.5 ml deionized water to obtain solution A. 0.7605 ml solution B, which containing $3.266{\cdot}10^{-3}$ mol ammonium persulfate (oxidizing agent) and $1.633{\cdot}10^{-3}$ mol phytic acid (cross-linking agent), was added into the above mixture. 2 min later, the color of solution changed from brown to dark green. Moreover, the solution became viscous and gel-like, suggesting that pyrrole monomer polymerized to form the PPy hydrogel. Secondly, the composite hydrogel was purified by dialysis for 2 days to remove inorganic salts and soluble monomer/oligomer. Finally, the composite was freeze dried overnight.

The obtained samples were characterized by the X-ray diffraction (XRD, D/max 2500PC). The morphology features were investigated by transmission electron microscopy (TEM, JEM-2100) and field emission scanning electron microscopy (FESEM, SUPRA55). FTIR Spectra were carried out on the NICOLET 560 Fourier transform infrared spectrophotometer.

The electrode was made of 80 wt% as-prepared material, 10 wt% Super-P, and 10% sodium carboxymethyl cellulose (CMC). The mixture slurry was prepared by using ultrapure water as a solvent, then uniform bladed on pure copper foil current collector via doctor blade processing and

dried under vacuum at 105℃ for 12 h. The cells were prepared in an argon-filled glovebox, using 1 M $LiPF_6$ in a mixture of ethylene carbonate, dimethyl carbonate, and ethyl methyl carbonate in 1:1:1 (V/V/V) ratio with 10 wt% fluorinated ethylene carbonate (FEC) as the electrolyte, lithium foil as the counter electrode, Celgard 2400 as the separator. The cells were investigated in the potential range from 0.01 V to 2 V (vs. Li^+/Li) by CT2001A Land battery testing system.

3. RESULTS AND DISSCUSSION

3.1. Material characterization

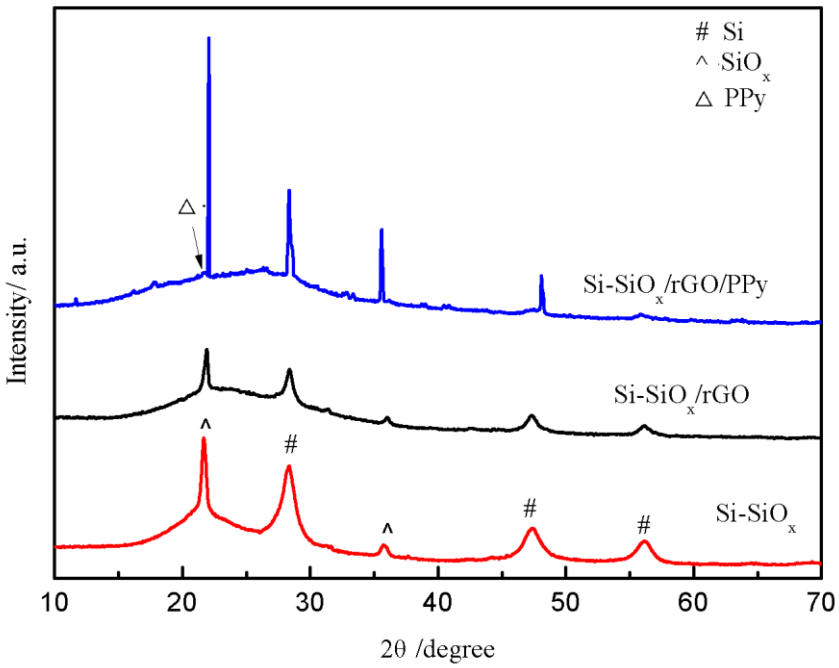

Figure 1. XRD patterns of Si-SiO_x , Si-SiO_x/rGO and Si-SiO_x/rGO/PPy

The X-ray diffraction (XRD) curves of Si-SiO_x, Si-SiO_x/rGO and Si-SiO_x/rGO/PPy composites are described in Fig. 1. The peaks at around 28.5°. 47.5° and 56° in Si-SiO_x and Si-SiO_x/rGO composites associated with the characteristic diffraction of Si [23,24]. The peaks at around 22° and 35° and in Si-SiO_x and Si-SiO_x/rGO composites correspond to the characteristic diffraction of SiO_x [25,26]. The peak appears at 12° corresponding to the characteristic diffraction of GO was no longer observed in Si-SiO_x/rGO composite, indicating that GO was successfully reduced into the reduced graphene oxide (rGO) [27,28]. It can be seen from the Si-SiO_x/rGO/PPy composite spectra that a relatively weak peak at 23.5° is observed, which associated with the characteristic diffraction of PPy, indicating in-situ polymerization of PPy coating on the surface of Si-SiO_x/rGO particles [29,30].

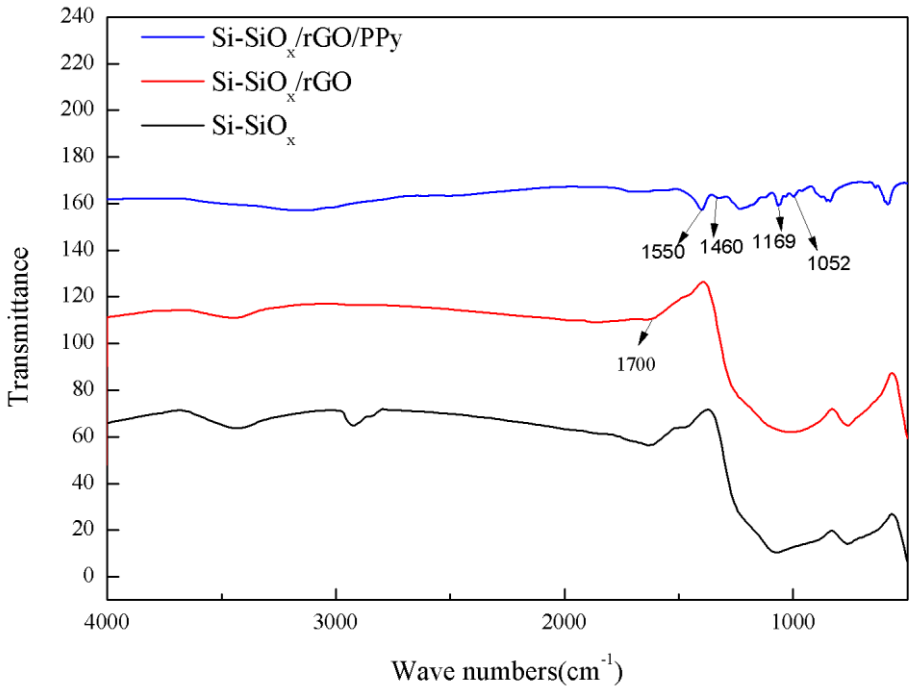

Figure 2. Infrared spectroscopy of Si-SiO$_x$, SiO$_x$/rGO, Si-SiO$_x$/rGO/PPy

The Infrared spectroscopy (IR) curves of Si-SiO$_x$, Si-SiO$_x$/rGO and Si-SiO$_x$/rGO/PPy composites are shown in Fig. 2 The peak appears at around 1700 cm-1 corresponding to the characteristic diffraction of GO is disappeared in Si-SiO/rGO composite, indicating that GO was reduced into reduced graphene oxide [31], which is in accordance with the XRD results. As clearly seen from the spectrum of Si-SiO$_x$/rGO/PPy composite, the characteristic peaks at 1460 and 1550 cm^{-1} are attributed to C-N and C=C stretching vibration in the ring of PPy are observed. The existence of peak at 1169 cm^{-1} is assigned to the vibration of the pyrrole ring. In addition, the peak at 1169 cm^{-1} corresponding to C-H the plane bending [30,32]. The above results verify that the successful polymerization of PPy coating on the surface of Si-SiO$_x$/rGO particles.

Scanning electron microscopy of Si-SiO$_x$, Si-SiO$_x$/rGO and Si-SiO$_x$/rGO/PPy composites are shown in Fig 3a-c. Fig. 3a reveals that Si-SiO$_x$ particles possess a diameter of 1~10 μm. Fig. 3b describes that Si-SiO$_x$ particles deposited on the surface of rGO. Fig. 3c demonstrates that the dried polymer hydrogel formed three dimensional porous foam-like network consisting of dendritic nanofibers with diameters of ~1 μm, and Si-SiO$_x$ composite embedded inside the porous polymer matrix. The TEM images of Si-SiO$_x$, Si-SiO$_x$/rGO, Si-SiO$_x$/rGO/PPy are shown in Fig. 3d-f. It can be seen from Fig. 3e that Si-SiO$_x$ particles deposited on the surface of rGO. Fig. 3f reveals that Si-SiO$_x$/rGO particles are be encapsulated by a conformal PPy due to the in-situ polymerization process. The TEM results agree well with the SEM results.

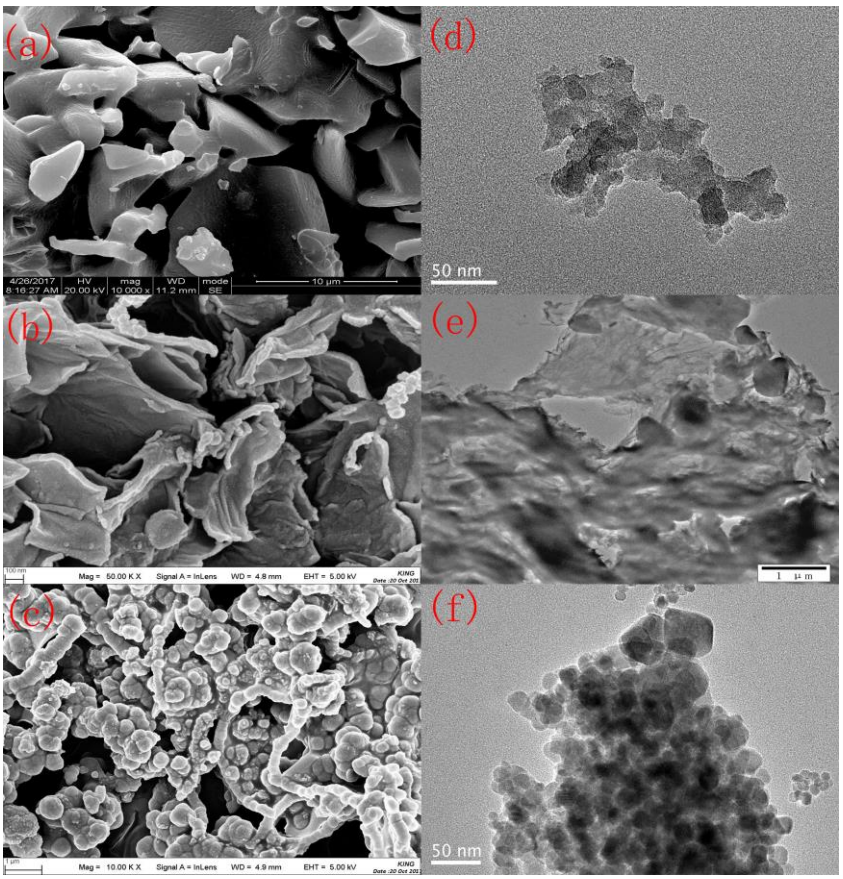

Figure 3. SEM images of samples: SiO_x-Si (a), SiO_x-Si/G (b), PPy/G/SiO_x-Si composites (c), TEM images of samples: SiO_x-Si (d), SiO_x-Si/G (e) and PPy/G/SiO_x-Si composites (f)

3.2. Electrochemical properties

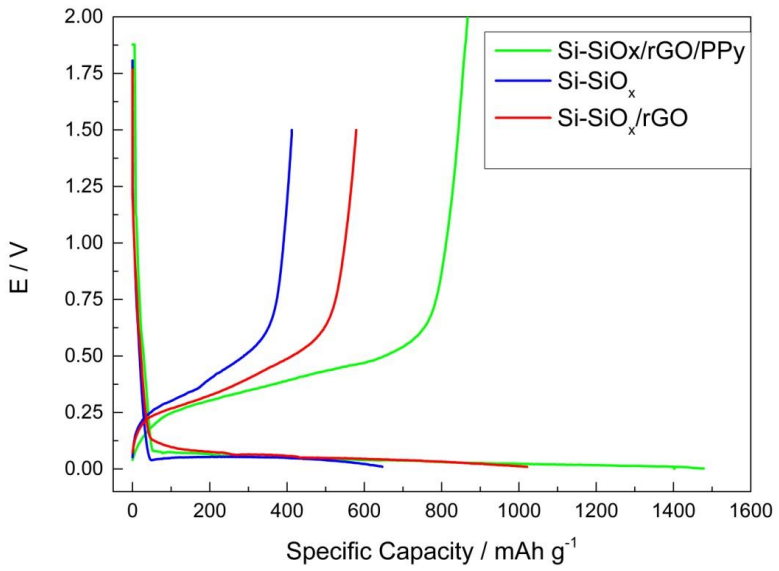

Figure 4. (a) Charge-discharge profiles of Si-SiO_x, SiO_x/rGO, Si-SiO_x/rGO/PPy

The charge-discharge profiles for Si-SiO_x, Si-SiO_x/rGO and Si-SiO_x/rGO/PPy composites in the first cycle are described in fig. 4a. The initial reversible capacities of Si-SiO_x, Si-SiO_x/rGO and Si-SiO_x/rGO/PPy are 646.7, 1021.3 and 1478.3 mAh·g^{-1}, respectively. And the correspoding initial charge-discharge efficiencies are 53%, 56.6% and 58.6%, respectively.

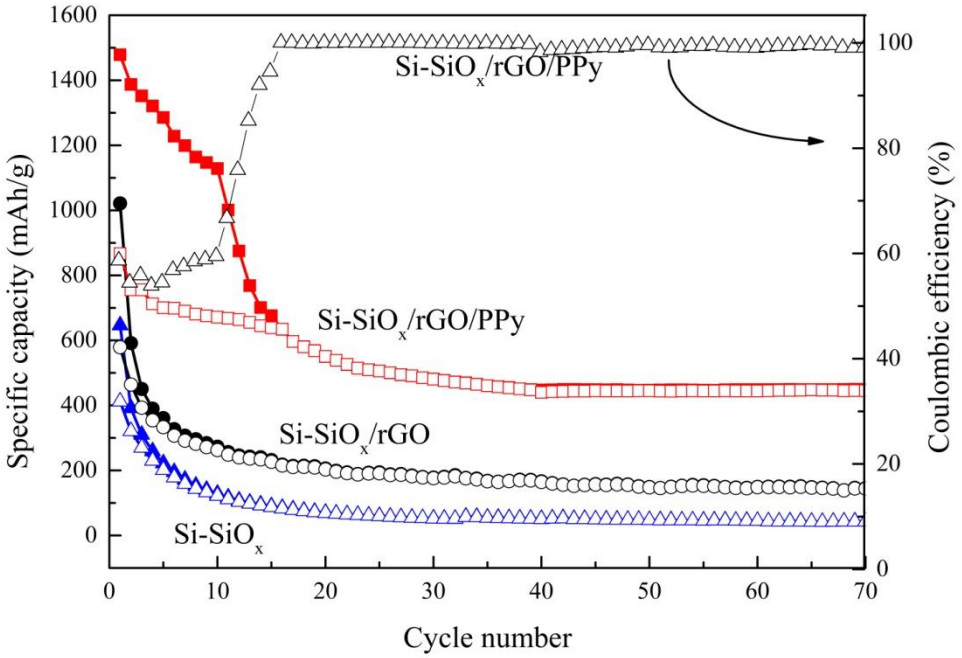

Figure 4. (b) Cycle performance profile pattern of Si-SiO_x-cristobale, Si-SiO_x/rGO, Si-SiO_x/rGO/PPy

The cycling properties of Si-SiO_x, Si-SiO_x/rGO, Si-SiO_x/rGO/PPy composites was studied at a current density of 0.1 A·g^{-1} in the potential range from 0.01 V to 2 V, and the results are given in Fig.4b. As illustrated, the reversible lithium capacity of Si-SiO_x is 646.7 mAh•g^{-1} in the initial cycle, and only 7.8% of its capacity is remained after 70 cycles. The low reversible lithium capacity and poor cycling stability of Si-SiO_x could be attributed to its poor conductivity and huge stress induced by volume expansion during cycling process [33]. In comparison with Si-SiO_x composite, Si-SiO_x/rGO possesses much higher initial reversible capacity of 1021.3 mAh•g^{-1} and improved capacity retention ratio of 14.6%, suggesting that introduction of rGO into Si-SiO_x composite can increase the conductivity of Si-SiO_x and lithium ion transfer as well as decrease the volume variations during the charge-discharge process [34]. Compared with Si-SiO_x/rGO composite, Si-SiO_x/rGO/PPy composite exhibits increased reversible capacity of 1478.3 mAh•g^{-1} in the initial cycle and higher capacity retention ratio of 30.4%, reflecting that dried polymer hydrogel formed three dimensional porous foam-like network, which provides a continuous conductive framework to shorten the electron and ion transport length. In addition, PPy coating on the surface of Si-SiO_x composite offers structural stability of Si-based materials [35,36].

The coulombic efficiency (CE) of Si-SiO_x/rGO/PPy composite is described in Fig.4a. As seen from Fig.4b, the coulombic efficiency in the first cycle is about 58.6%. The low initial coulombic

efficiency might be due to the decomposition of electrolytes and formation of SEI film on the electrode surface and reduction of SiO_x [33,37]. But the average coulombic efficiency from the 15th to 70th cycle increases to 99.8%.

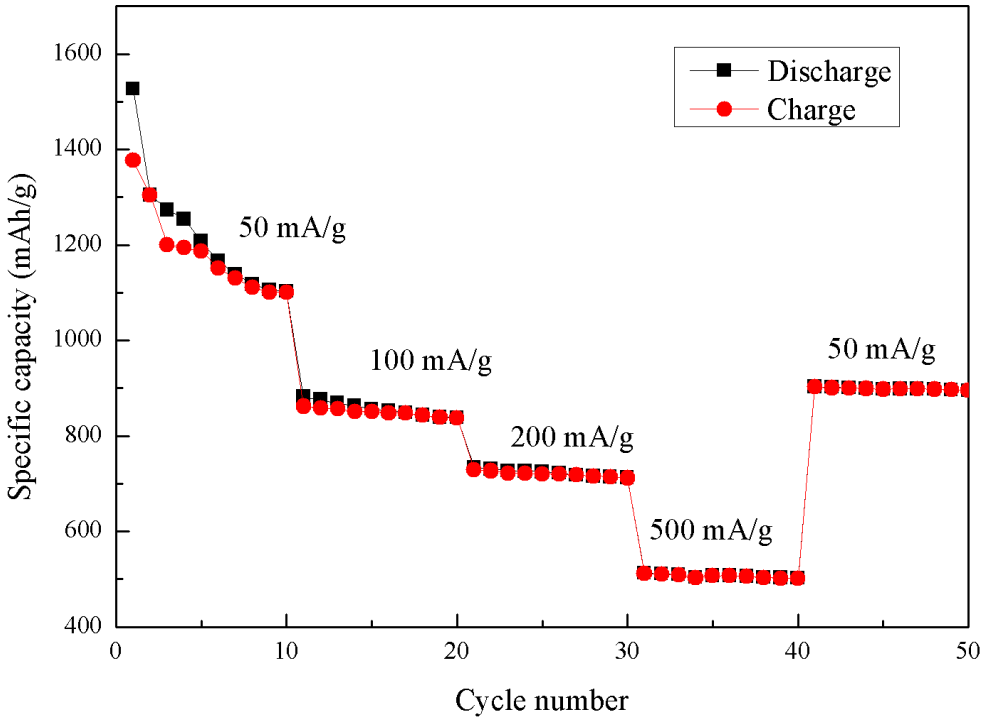

Figure 4. (c) Rate capability of Si-SiO_x/rGO/PPy composite

Rate performance of Si-SiO_x/rGO/PPy composite was investigated at different current densitiesranging from 50 mA/g to 500 mA/g, and then back to 50 mA/g, and the results are described in Fig.4c. Clearly, Si-SiO_x/rGO/PPy composite exhibits a reversible capacity of 1500 mAh/g, 850 mAh/g, 720 mAh/g and 500 mAh/g at 50 mA/g, 100 mA/g, 200 mA/g and 200 mA/g, respectively. As the current density returns to 50 mA/g even after 40 cycles at various current densities, the reversible capacity is 894 mAh/g. the above results demonstrated that Si-SiO_x/rGO/PPy composite possesses good rate capability.

Table 1 compares the results of other Si-based materials with the current study. Clearly, Si-SiO_x/rGO/PPy exhibits much better electrochemical performance. The superior performance of Si-SiO_x/rGO/PPy composite could be attributed to the following reasons: (1) fabrication of Si-SiO_x composites can greatly improve its cycle performances, owing to the in situ generated Li_2O during the first discharge process, which can inhibit the volume changes of silicon particles during the charge-discharge process [23,25,38,39]. (2) rGO provides a good electrical contact for Si-SiO_x materials as well as buffer its volume variations during the charge-discharge process [23,42]. (3) Dried polymer hydrogel formed three dimensional porous foam-like network, which provides a continuous conductive framework to shorten the electron and ion transport length [29,30].

Table 1. Comparison of the initial discharge performance of MR-Si/G, Si/C and Si-SiO_x/rGO/PPy

Sample	Charge/discharge current ($mA \cdot g^{-1}$)	Discharge capacity ($mAh \cdot g^{-1}$)	Reference
MR-Si/G	100	915	40
Si/C	100	602	41
SiO_x-CNFs	100	728.1	43
Si-SiO_x/Cr/C	100	810	44
Si-SiO_x/rGO/PPy	100	1478.3	Current study

4. SUMMARY AND CONCLUSION

Si-SiO_x/rGO/PPy composite is successfully fabricated via in-situ polymerization process. For comparison, the electrochemical performance of Si-SiO_x, Si-SiO_x/rGO is also investigated. The results demonstrated that Si-SiO_x/rGO/PPy composite shows the best performance among the three samples. The superior performance can be attributed to that rGO provides a good electrical contact for Si-SiO_x materials as well as buffer its volume variations during the charge-discharge process, and PPy gel provides a continuous conductive framework to shorten the electron and ion transport length.

ACKNOWLEDGEMENTS
This project was financially supported by the National Nature Science Foundation of China (No.21576030 and U1607127)，the Natural Science Foundation of the Jiangsu Higher Education Institutions of China (No. 15KJA150002), the Priority Academic Program Development of Jiangsu Higher Education Institutions (PAPD) and Qing Lan Project of Education Department of Jiangsu Province.

References

1. J. H. Ryu, J. W. Kim, Y. Sung, S. M. Oh, *Electrochem. Society. Solid-State. Lett.*, 7 (2004) 306.
2. H. Wu, G. Chan, J.W. Choi, I. Ryu, Y. Yao, M. T. McDowell, S. W. Lee, A. Jackson, Y. Yang, L. Hu, Y. Cui, *Nat. nanotechno.*, 7 (2012) 310.
3. W. Xu, S. S. S. Vegunta, J. C. Flake, *J. Power. Sources*, 196 (2011) 8583.
4. M. Ge, J. Rong, X. Fang, C. Zhou, *Nano Lett*., 12 (2012) 2318.
5. B. M. Bang, J. Lee, H. Kim, J. Cho, S. Park, *Adv. Energy. Mater.*, 2 (2012) 878.
6. Y. Zhao, X. Liu, H. Li, T. Zhai, H. Zhou, *Chem. Commun.*, 48 (2012) 5079.
7. L. Shen, X. Guo, X. Fang, Z. Wang, L. Chen, *J. Power Sources*, 213 (2012) 229.
8. S. Son, S. C. Kim, C. S. Kang, T.A. Yersak, Y. Kim, C. Lee, S. Moon, J.S. Cho, J. Moon, K. H. Oh, S. Lee, *Adv. Energy. Mater.*, 2 (2012) 1226.
9. Y. S. Hu, R. D. Cakan, M. M. Titirici, J. O. M. R. Schl, M. Antonietti, J. Maier, Angew, *Chem. Int. Edit.*, 47 (2008) 1645.
10. T. Hasegawa, S. R. Mukai, Y. Shirato, H. Tamon, *Carbon*, 42 (2004) 2573.
11. Y. Liu, K. Huang, Y. Fan, Q. Zhang, F. Sun, T. Gao, Z. Wang, J. Zhong, *Electrochim. Acta*, 102 (2013) 246.
12. S. L. Wei, Z. Zhen, R. Manman, *Chem. Commun.*, 46 (2010) 2590.
13. H. Guo, R. Mao, X. Yang, J. Chen, *Electrochim. Acta*, 74 (2012) 271.
14. X. Xin, X. Zhou, F. Wang, X. Yao, X. Xu, Y. Zhu, *J. Mater. Chem.*, 22 (2012) 7724.

15. Y. S. Hu, R. Demir-Cakan, M. M. Titirici, J. O. Muller, S. Robert, A. Markus, *Angew. Chem. Int.* Ed., 47 (2008) 1645.
16. Y. X. Xu, Z. Lin, X. Zhong, X. Q. Huang, N. O. Weiss, Y. Huang, X. F. Duan, *Nat. Commun.*, 5 (2014) 4554.
17. G. Eda, G. Fanchini, M. Chhowalla, *Nat. Nanotechnol.*, 3 (2008) 270.
18. J. Wang, H.vY. Lü, C.vY. Fan, F. Wan, J. Z. Guo, Y.Y. Wang, X. L. Wu, *J. Alloy Compd.*, 694 (2017) 208.
19. D. Ji, Z. W. Yang, L. L. Xiong, H. L. Luo, G. Y. Xiong, Y. Zhu, Y. Z. Wan, *RSC. Adv.*, 7 (2017) 4209.
20. Z. M. Bai, F. X. Liu, J. Liu, Y. H. Zhang, *J. Mater. Sci.*, 52 (2017) 10497.
21. M. W. Verbrugge, Y. T. Cheng, *Electrochem. Soc. Trans.*, 13 (2008) 127.
22. M. W. Verbrugge, Y. T. Cheng, *J. Electrochem. Soc.*, 156 (2009) 927.
23. X. Y. Tie, Q. Y. Han, C. Y. Liang, B. Li, J. T. Zai, X. F. Qian, *Front. Mater.*, 4 (2018) 47.
24. J. Niu, S. Zhang, Y. Niu, H. H. Song, X. H. Chen, J. S. Zhou, B. Cao, *RSC. Adv.*, 3 (2015) 19892.
25. Y. R. Ren, M. Q. Li, *Electrochim. Acta*, 142 (2014) 11.
26. L. Z. Qian, J. L. Lan, M. Y. Xue, Y. H. Yu, X. P. Yang, *RSC. Adv*, 7 (2017) 36697.
27. H. C. Tao, L. Y. Xiong, S. C. Zhu, L. L. Zhang, X. L. Yang, *J. Electroanal. chem.*, 12 (2017) 16.
28. X. J. Bai, Y. Y. Yu, H. H. Kung, B. Wang, J. M. Jiang, *J. Power Sources*, 306 (2016) 42.
29. C. L. Li, C. Liu, Z. Mutlu, Y. Yan, K. Ahmed, M. Ozkan, C. S. Ozkan, *RSC. Adv.*, 7 (2017) 36541.
30. C. L. Li, C. Liu, K. Ahmed, Z. Mutlu, Y. Yan, L. Lee, M. Ozkan, C. S. Ozkan, *MRS Adv.*, 7 (2017) 3323.
31. H. Li, L. F. Liu, F. L. Yang, *J. Mater. Chem. A*, 1 (2013) 3446-3453.
32. Q. T. Wang, R. R. Li,D. Yu, X. Z. Zhou, J. Li, Z. Q. Lei, *RSC Adv.*, 4 (2014) 54134.
33. H. Liu, Y. J. Zou, L. Y. Huang, H. Yin, C. Q. Xi, X. Chen, H. W. Shentu, C. Li, J. J. Zhang, C. J. Lv, M. Q. Fan, *Appl. Surf. Sci.*, 442 (2018) 204.
34. H. Tang, J. P. Tu, X. Y. Liu, Y. J. Zhang, S. Huang, W. Z. Li, X. L. Wang, C. D. Gu, J. *Mater. Chem. A.*, 2 (2014) 5834.
35. J. Li, J. G. Huang, *Chem. Commun.*, 51 (2015) 14590.
36. Z. J. Du, S. C. Zhang, Y. Liu, J. F. Zhao, R. X. Liu, T. Jiang, J. *Mater. Chem.*, 22 (2012) 11636.
37. N. H. Yang, Y. S. Wu, J. Chou, H. C. Wu, N. L. Wu, *J. Power Sources*, 296 (2015) 314.
38. S. J. Lee, H. J. Kim, T. H. Hwang, S. H. Choi, S. H. Park, E. Deniz, D. S. Jung, J. W. Choi, *Nano lett.*, 17 (2017) 1870.
39. Y. F. Chen, Y. F. Lin, N. Du, Y. G. Zhang, H. Zhang, D .R. Yang, *Chem. Commun.*, 45 (2017) 6101.
40. J. L. Zhu, Y. R. Ren, B. Yang, W. K. Chen, J. N. Ding, *Nanoscale res. Lett.*, 12 (2017) 627.
41. Z. W. Yang, Y. Yang. H. J. Guo, Z. X. Wang, X. H. Li,Y. Zhou, J. X. Wang, *Ionics*, 4 (2018) 1-7
42. X. H. Li, M. Q. Wu, T. T. Feng, Z. Q. Xu, J. G. Qin, C. Chen, C. Y. Tu, D. X. Wang, *RSC Adv.*, 7 (2017) 48286.
43. X.D. Yan, D. H. Teng, X. L. Jia, Y. H. Yu, X. P. Yang, *Electrochim. Acta*, 108 (2013) 196.
44. M. Q. Li, J. W. Gu, X. F. Feng, H. Y. He, C. M. Zeng, *Electrochim. Acta*, 164 (2015) 163.